Proceedings of the 28th IEEE
EMBS Annual International Conference
New York City, USA, Aug 30-Sept 3, 2006

Estimation of Arterial Wall Strain Based on IVUS Image Registration

Yun Liang, Kevin D. Oakeson, Hui Zhu, and Morton H. Friedman

Abstract—**In this study, we propose a method to estimate arterial wall strain using intravascular ultrasound (IVUS) images. The method is based on a nonrigid image registration algorithm, which represents the displacement field by cubic B-splines, and incorporates smoothness and incompressibility constraints. The 2D displacement field is then used to calculate the local strain tensors. With the 2D strain tensors, both radial and circumferential strain distributions can be obtained, and color-coded for display. The algorithm has been evaluated with synthetic motion IVUS images and phantom IVUS images under two luminal pressures.**

I. INTRODUCTION

Atherosclerotic plaque rupture is responsible for the majority of myocardial infarctions and acute coronary syndromes. The mechanical behavior of the plaque is dependent on its geometry and composition [1]. Currently, intravascular ultrasound (IVUS) imaging is the only clinically available technique capable of providing real-time cross-sectional images of the arterial anatomy with excellent spatial representation of atherosclerotic plaque [2]. However, the capability to identify different plaque components is still limited in B-mode IVUS images [3].

Introduced in the late nineties, IVUS elastography is a technique that reveals vascular elastic properties by measuring radial strain through correlation analysis of radiofrequency (r. f.) ultrasound signals recorded at different intraluminal pressures [4, 5]. However, reliable strain estimates are only obtained when the tissue motion is aligned with the r. f. signal direction and the r. f. traces at low and high pressure correspond to the tissue at the same circumferential position. These are difficult to overcome due to the movements of the IVUS catheter [6], which are mostly introduced by cardiac motion, and non-uniform tissue deformation. Although some researchers used 2D correlation windows [7], or implemented angle matching before correlation [8], this issue is not well resolved. Furthermore, IVUS elastography based on 1D r. f. signal correlation only characterizes the radial strain.

Non-rigid image registration has been widely used in medical image analysis [9]. It has received little attention in the study of IVUS elastography, although to detect the motion between two IVUS images is a typical image registration problem. Since image registration can be used to measure global and local displacements in both the circumferential and radial directions, a comprehensive 2D strain field can be obtained at each local point.

The aim of this study is to enhance the IVUS elastography technique using nonrigid image registration methods, a processing method in 2D, and to evaluate the accuracy of the estimated arterial wall strain. In Section II, we first describe a non-rigid image registration algorithm based on the cubic B-spline representation of the displacement field. Then the 2D strain tensor is determined from the deformation matrix, which is derived from the displacement field. In Section III, the study design and experimental setup used to generate test image data are presented. In Section IV, the evaluation results from IVUS images with synthetic motions, and results from a homogeneous vessel-mimicking phantom study are reported.

II. METHODS

A. Image Registration Algorithm

Non-rigid image registration is generally formulated as an optimization problem, whose goal is to minimize an associated cost function. In this study, the proposed cost function is a combination of a term that characterizes the similarity between reference and target images, and weighted terms that add robustness to motion estimation by incorporating a tissue incompressibility assumption and displacement smoothness constraint.

Since we are considering cylindrical-like geometries, we perform the image registration in polar coordinates with the origin at the centroid of the lumen. This also simplifies the computation. Alignment of the lumen centroids in the two images before the registration can help overcome any lateral movement of the catheter between images. Image segmentation of the vessel wall area is performed to locate the lumen centroid and define the region of interest (ROI) for registration. The lumen and media-adventitia borders are identified using a "B-snakes" method [10]. The displacement field and strain tensor are calculated in polar coordinates. Finally, the strain distribution is transformed into Cartesian coordinates for display.

The overall cost function of the image registration is:

Manuscript received April 21, 2006. This work is supported in part by the NIH Grant R01-058856.

Yun Liang, Hui Zhu, and Morton H. Friedman are with Department of Biomedical Engineering, Duke University, Durham, NC 27708-0281 USA (phone: 919-660-5125; fax: 919-648-4488; e-mail: yl18@duke.edu).

Kevin D. Oakeson, was with Department of Biomedical Engineering, Duke University, Durham, NC 27708 USA. He is now with Medtronic Richmond District, Richmond, VA USA (email: kevin.d.oakeson@medtronic.com)

$$E(D(r_i,\theta_i)) = E_{IS}(D(r,\theta_i)) + \alpha E_{IC}(D(r_i,\theta_i)) + \beta E_{SC}(D(r,\theta_i)) \quad (1)$$

This cost function depends on the displacement field $D(r_i,\theta) = [u(r_i,\theta_i), v(r_i,\theta_i)]$, with $u(r_i,\theta_i)$ and $v(r_i,\theta_i)$ representing the displacements in radial and circumferential directions, respectively. The image intensity similarity is measured by:

$$E_{IS}(D(r_i,\theta_i)) = \frac{1}{N}\sum_i [I_1(r_i+u_i,\theta_i+v_i) - I_0(r_i,\theta_i)]^2 \quad (2)$$

The incompressibility constraint term is defined as:

$$E_{IC}(D(r,\theta)) = \int \|\nabla \bullet D(r,\theta)\|^2 dr d\theta \quad (3)$$

And the strain smoothness constraint term is defined as:

$$E_{SC}(D(r,\theta)) = \int\left(\frac{\partial^2 D}{\partial r^2} + \frac{\partial^2 D}{\partial \theta^2} + 2\left(\frac{\partial^2 D}{\partial r \partial \theta}\right)\right) dr d\theta \quad (4)$$

The transformation model is formulated as a free-form deformation based on cubic B-splines [11, 12]. The displacements are represented as two-dimensional B-splines controlled by a small number of control points $\hat{u}_j$ and $\hat{v}_j$ which lie on a coarser B-spline grid:

$$u(r_i,\theta_i) = \sum_j \hat{u}_j B_j(r_i,\theta_i) = \sum_j \hat{u}_j \omega_{ij}$$
$$v(r_i,\theta_i) = \sum_j \hat{v}_j B_j(r_i,\theta_i) = \sum_j \hat{v}_j \omega_{ij} \quad (5)$$

where the $B(r_i,\theta_i)$ is the cubic B-spline basis function. For each pixel, the displacement is computed from the surrounding 4×4 neighborhood of control points.

We use the adapted Levenberg-Marquardt iterative non-linear minimization technique to recover the spline-based transformation model parameters, which are the displacements at the control points [11, 13].

In order to handle a large deformation field, avoid a local minimum pitfall and save computational resources, we run the algorithm in a multi-resolution fashion [14]. A Gaussian image pyramid is computed. We first run the algorithm on one of the coarser pyramid levels, and use the resulting deformation estimates to initialize the next finer level of registration.

B. Strain Computation

Following the displacement field estimation, the deformation matrix *F* in polar coordinates is computed [15]:

$$F = \begin{bmatrix} \frac{\partial u}{\partial R} & \frac{1}{R}\frac{\partial u}{\partial \Theta} \\ r\frac{\partial v}{\partial R} & \frac{r}{R}\frac{\partial v}{\partial \Theta} \end{bmatrix} \quad (6)$$

The deformation matrix is related to the strain tensor by

$$E = \begin{bmatrix} \varepsilon_{rr} & \varepsilon_{r\theta} \\ \varepsilon_{r\theta} & \varepsilon_{\theta\theta} \end{bmatrix} = \frac{1}{2}F^T F - I \quad (7)$$

where I is the identity matrix.

The radial strain ε_{rr} and circumferential strain $\varepsilon_{\theta\theta}$ are color coded, and each is plotted as a 2D image in Cartesian coordinates congruent with the lumen perimeter.

III. Experimental Design

In order to evaluate the performance of the image registration algorithm, we have developed an experimental setup based on a clinical IVUS system (ClearView, Boston Scientific) and a custom-designed vessel holding apparatus. The central frequency of the IVUS catheter (Atlantis SR Pro, Boston Scientific) is 40 MHz. The experimental specimens are polyvinyl alcohol (PVA) cryogel phantoms [16] or excised porcine carotid arteries. The intraluminal pressure is manipulated using a computer-controlled air valve (Proportion-Air IN). The intraluminal pressure is monitored with a pressure transducer (ISOTEC, Harvard Apparatus).

To evaluate the image registration algorithm, we applied a known displacement field to an IVUS image of a porcine carotid artery to generate synthetic test image data. The known displacements are based on the deformation model for a thick-walled cylinder [17]. The deformation model can be simplified as the displacements in the radial and circumferential directions, respectively:

$$U(r) = \frac{B}{r}$$
$$V(r) = 0 \quad (8)$$

where *B* is related to the elastic properties of the artery wall, and can be characterized by the circumferential elastic modulus and Poisson's ratio. In our experiments, *B* was assigned a value so that the radial displacement at the minimum radius point of the lumen border was 5%. Then the rest of the pixels were moved radially outwards according to Eq. (8). Image registration was performed between the original IVUS image and its deformed version.

Image noise was not considered in the above experiment. Instead of adding a certain kind of noise, such as Gaussian noise to the deformed image, a second IVUS image of the same porcine carotid artery was captured at the same location and under the same luminal pressure. We registered this image to the former artificially deformed image to test the robustness of the algorithm against image noise.

In addition to using artificially deformed images to demonstrate the performance of our image registration algorithm, we also applied the algorithm to a pair of IVUS images acquired at the same location in a homogeneous, concentric tissue-equivalent phantom. The phantom is cylindrical, with inner and outer diameters of 3 and 18 mm, respectively, and a length of 8 cm. The phantom is made from 10% weight PVA cryogel through 3 freeze-and-thaw cycles. The images were captured at two intraluminal pressures with 24 mm Hg difference.

IV. Results

Fig.1 shows (a) an IVUS image of a porcine carotid artery, and (b) a synthetic image obtained after the

displacement field described in Eq. (8) is applied to image (a). In both images, the lumen and media-adventitial boundaries were identified and the centroids of the lumens were obtained.

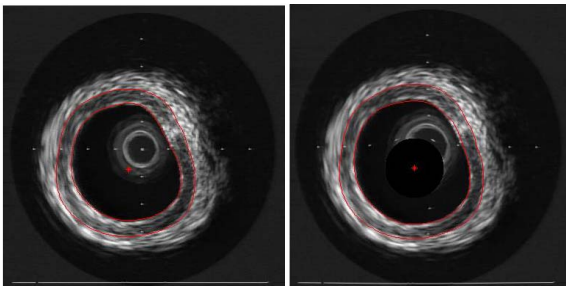

(a) (b)

Fig.1 (a) an IVUS image of a pig carotid artery; (b) artificially pressurized form of image (a) with known displacements.

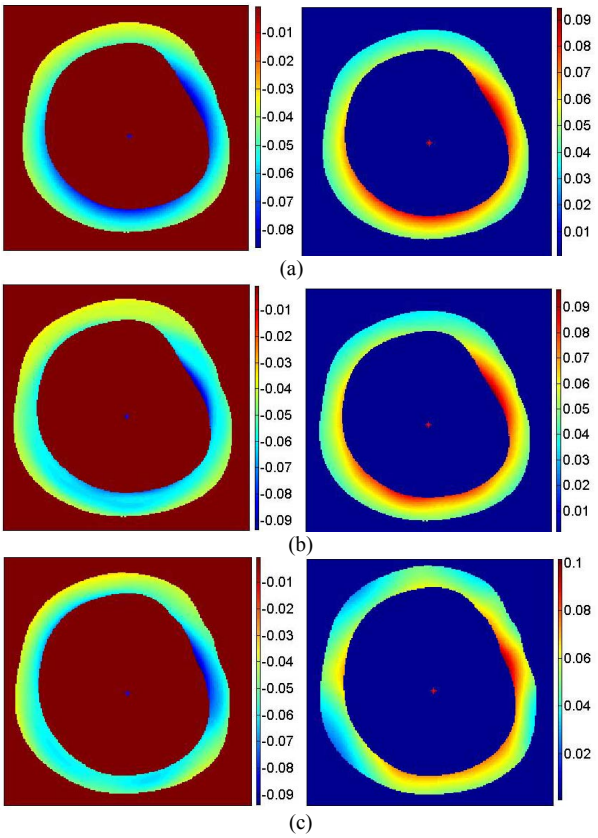

Fig.2 Results of the artificial deformation experiments, radial strains on the left and circumferential strains on the right: (a) theoretical strain distributions generated by the applied displacements; (b) strain distributions calculated by registering an image to its deformed version; (c) strain distributions calculated by registering an image to another image's deformed version.

Fig. 2 demonstrates the evaluation test results. Fig 2a shows the radial and circumferential strain distributions corresponding to the applied displacement fields. Fig. 2b shows the radial and circumferential strain distributions calculated from the registration between the image (fig. 1a) and its deformed version (fig. 1b). The correlation coefficients between the theoretical and calculated strain values are 0.96 for the radial strain and 0.99 for circumferential strain. Fig. 1c demonstrates the calculated strain results between the second IVUS image described earlier and fig. 1b. The second image was captured at the same site and the same luminal pressure as fig. 1a. The correlation coefficients between the theoretical and calculated strain values in this case are 0.87 radially and 0.85 circumferentially. Because the lumen is not circular, all the strain distributions shown in Fig. 2 do not look axis symmetric.

As the vessel expands under the increment of luminal pressure, the wall is compressed in the radial direction yielding negative strain values, while the tissue is stretched in the circumferential direction, giving positive strain values.

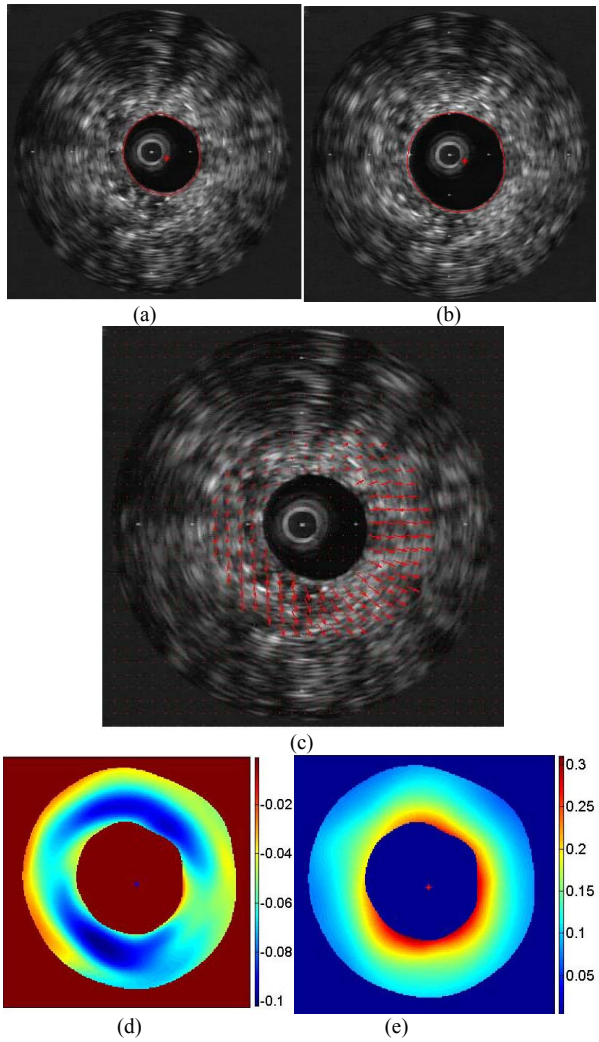

Fig.3 Experimental results for a PVA cryogel phantom: (a) image before deformation; (b) image after deformation; (c) displacement field obtained by registration of (a) to (b); (d) radial strain distribution and (e) circumferential strain distribution.

Fig. 3 shows the deformation of a homogeneous, concentric PVA cryogel vessel phantom in response to incremental luminal pressure of 24 mmHg. The vector field, shown in fig. 3c, is the 2D displacement field from the

registration results. Both the displacement field and strain distributions cover the vessel wall area extending about 2.7 mm from the lumen in the radial direction. The displacement vector field shows that the motion between 2 and 7 o'clock is dominant during the phantom expansion. This is because the lumen of the phantom is not perfectly circular and the phantom bends slightly when it is pressurized. The absolute values of both the radial and circumferential strain decay with the radial distance. This decay stems from the stress distribution. The strain values in both directions are virtually azimuthally symmetric, consistent with the phantom being homogeneous and concentric.

V. DISCUSSION AND CONCLUSION

We have presented a new method for estimation of arterial wall strain based on nonrigid image registration of IVUS images. Both radial and circumferential strains can be obtained by this method. The circumferential strain may provide more information than radial strain alone in studying the arterial wall mechanics

Due to the speckle nature of the B-mode IVUS images, image registration based on intensity similarity could be very challenging. The experimental results indicate that the strain smoothness constraint and tissue incompressibility terms are effective and efficient. These two constraints are reasonable assumptions for soft tissue deformation. In addition, they, as well as the multi-resolution strategy, help the registration process avoid local minima. The multi-resolution strategy also reduces computation time.

With our method, the arterial wall strain analysis has been carried out in both radial and circumferential directions. Therefore, our motion analysis can detect larger strain compared to elastography techniques based on 1D signal correlation, which suffer from signal de-correlation when tissue motion is large. Even though the IVUS images carry less information than the r. f. signals from which they are generated, our image registration technique can detect tissue motion with high accuracy and sensitivity.

In conclusion, the presented study has shown the effectiveness of our image registration based method in estimation of arterial wall strain, which is promising for arterial tissue characterization based on conventional IVUS images.

ACKNOWLEDGMENT

This research is supported by NIH grant HL058856. We would like to thank Dr. David Long for his assistance in building the experimental setup and analysis of the mechanical properties of the thick wall model.

REFERENCE

[1] P. D. Richardson, "Biomechanics of plaque rupture: Progress, problems, and new frontiers," *Annals of Biomedical Engineering*, vol. 30, pp. 524-536, 2002.

[2] G. S. Mintz, S. E. Nissen, W. D. Anderson, S. R. Bailey, R. Erbel, P. J. Fitzgerald, F. J. Pinto, K. Rosenfield, R. J. Siegel, E. M. Tuzcu, and P. G. Yock, "American College of Cardiology Clinical Expert Consensus Document on Standards for Acquisition, Measurement and Reporting of Intravascular Ultrasound Studies (IVUS) - A report of the American College of Cardiology Task Force on Clinical Expert Consensus," *Journal of the American College of Cardiology*, vol. 37, pp. 1478-1492, 2001.

[3] S. E. Nissen and P. Yock, "Intravascular ultrasound - Novel pathophysiological insights and current clinical applications," *Circulation*, vol. 103, pp. 604-616, 2001.

[4] C. L. de Korte and A. F. W. van der Steen, "Intravascular ultrasound elastography: an overview," *Ultrasonics*, vol. 40, pp. 859-865, 2002.

[5] C. L. de Korte, S. G. Carlier, F. Mastik, M. M. Doyley, A. F. W. van der Steen, P. W. Serruys, and N. Bom, "Morphological and mechanical information of coronary arteries obtained with intravascular elastography - Feasibility study in vivo," *European Heart Journal*, vol. 23, pp. 405-413, 2002.

[6] A. Arbab-Zadeh, A. N. DeMaria, W. F. Penny, R. J. Russo, B. J. Kimura, and V. Bhargava, "Axial movement of the intravascular ultrasound probe during the cardiac cycle: Implications for three-dimensional reconstruction and measurements of coronary dimensions," *American Heart Journal*, vol. 138, pp. 865-872, 1999.

[7] B. M. Shapo, J. R. Crowe, R. Erkamp, S. Y. Emelianov, M. J. Eberle, and M. Odonnell, "Strain imaging of coronary arteries with intraluminal ultrasound: Experiments on an inhomogenous phantom," *Ultrasonic Imaging*, vol. 18, pp. 173-191, 1996.

[8] C. R. M. Janssen, C. L. de Korte, M. S. van der Heiden, C. P. Wapenaar, and A. F. W. van der Steen, "Angle matching in intravascular elastography," *Ultrasonics*, vol. 38, pp. 417-423, 2000.

[9] W. R. Crum, T. Hartkens, and D. L. G. Hill, "Non-rigid image registration: theory and practice," *The British journal of Radiology*, vol. 77, pp. S140-153, 2004.

[10] K. D. Oakeson, H. Zhu, and M. H. Friedman, "Quantification of cross-sectional artery wall motion with IVUS image registration," *Proceedings of SPIE Medical Imaging 2004: Ultrasonic Imaging and Signal Processing*, vol. 5373, pp. 119-130, 2004.

[11] R. Szeliski and J. Coughlan, "Spline-based image registration," *International Journal of Computer Vision*, vol. 22, pp. 199-218, 1997.

[12] T. Rohlfing, C. R. Maurer, D. A. Bluemke, and M. A. Jacobs, "Volume-preserving nonrigid registration of MR breast images using free-form deformation with an incompressibility constraint," *IEEE Transactions on Medical Imaging*, vol. 22, pp. 730-741, 2003.

[13] W. H. Press, B. P. Flannery, S. A. Teukolsky, and W.T. Vetterling, *Numerical Recipes in C: The Art of Scientific Computing*, 2nd ed. Cambridge, England: Cambridge University Press, 1992.

[14] P. J. Burt and E. H. Adelson, "The Laplacian Pyramid as a Compact Image Code," *IEEE Transactions on Communications*, vol. 31, pp. 532-540, 1983.

[15] J. D. Humphrey, *Cardiovascular Solid Mechanics: Cells, Tissues, and Organs*, New York: Springer, 2002.

[16] J. Fromageau, E. Brusseau, D. Vray, G. Gimenez, and P. Delachartre, "Characterization of PVA cryogel for intravascular ultrasound elasticity imaging," *IEEE Transactions on Ultrasonics Ferroelectrics and Frequency Control*, vol. 50, pp. 1318-1324, 2003.

[17] R. R. Archer, and N.H. Cook, *An Introduction to the Mechanics of Solids*, 2nd ed. New York: McGraw-Hill, 1978.